

3.5

Basic Methods for Image Restoration and Identification

Reginald L. Lagendijk
and Jan Biemond

Delft University
of Technology,
The Netherlands

1	Introduction.....	167
2	Blur Models	169
2.1	No Blur • 2.2 Linear Motion Blur • 2.3 Uniform Out-of-Focus Blur • 2.4 Atmospheric Turbulence Blur	
3	Image Restoration Algorithms.....	171
3.1	Inverse Filter • 3.2 Least-Squares Filters • 3.3 Iterative Filters • 3.4 Boundary Value Problem	
4	Blur Identification Algorithms.....	178
4.1	Spectral Blur Estimation • 4.2 Maximum Likelihood Blur Estimation	
	References.....	181

1 Introduction

Images are produced to record or display useful information. Due to imperfections in the imaging and capturing process, however, the recorded image invariably represents a degraded version of the original scene. The undoing of these imperfections is crucial to many of the subsequent image processing tasks. There exists a wide range of different degradations that need to be taken into account, covering for instance noise, geometrical degradations (pin cushion distortion), illumination and color imperfections (under/over-exposure, saturation), and blur. This chapter concentrates on basic methods for removing blur from recorded sampled (spatially discrete) images. There are many excellent overview articles, journal papers, and textbooks on the subject of image restoration and identification. Readers interested in more details than given in this chapter are referred to [2, 3, 9, 11, 14].

Blurring is a form of bandwidth reduction of an ideal image owing to the imperfect image formation process. It can be caused by relative motion between the camera and the original scene, or by an optical system that is out of focus. When aerial photographs are produced for remote sensing purposes, blurs are introduced by atmospheric turbulence, aberrations in the optical system, and relative motion between the camera and the ground. Such blurring is not confined to optical images, for example electron micrographs are corrupted by spherical aberrations of the electron lenses, and CT scans suffer from x-ray scatter.

In addition to these blurring effects, noise always corrupts any recorded image. Noise may be introduced by the medium through which the image is created (random absorption or scatter effects), by the recording medium (sensor noise), by measurement errors due to the limited accuracy of the recording system, and by quantization of the data for digital storage.

The field of *image restoration* (sometimes referred to as image deblurring or image deconvolution) is concerned with the reconstruction or estimation of the uncorrupted image from a blurred and noisy one. Essentially, it tries to perform an operation on the image that is the inverse of the imperfections in the image formation system. In the use of image restoration methods, the characteristics of the degrading system and the noise are assumed to be known *a priori*. In practical situations, however, one may not be able to obtain this information directly from the image formation process. The goal of *blur identification* is to estimate the attributes of the imperfect imaging system from the observed degraded image itself prior to the restoration process. The combination of image restoration and blur identification is often referred to as *blind image deconvolution* [11].

Image restoration algorithms distinguish themselves from image *enhancement* methods in that they are based on models for the degrading process and for the ideal image. For those cases where a fairly accurate blur model is available, powerful restoration algorithms can be arrived at. Unfortunately, in numerous practical cases of interest the modeling of the blur

is unfeasible, rendering restoration impossible. The limited validity of blur models is often a factor of disappointment, but one should realize that if none of the blur models described in this chapter are applicable, the corrupted image may well be beyond restoration. Therefore, no matter how powerful blur identification and restoration algorithms are, the objective when capturing an image undeniably is to avoid the need for restoring the image.

The image restoration methods that are described in this chapter fall under the class of *linear spatially invariant restoration filters*. We assume that the blurring function acts as a convolution kernel or *point-spread function* $d(n_1, n_2)$ that does not vary spatially. It is also assumed that the statistical properties (mean and correlation function) of the image and noise do not change spatially. Under these conditions the restoration process can be carried out by means of a linear filter of which the point-spread function is spatially invariant, i.e., is constant throughout the image. These modeling assumptions can be mathematically formulated as follows. If we denote by $f(n_1, n_2)$ the desired ideal spatial discrete image that does not contain any blur or noise, then the recorded image $g(n_1, n_2)$ is modeled as (see also Fig. 1(a)) [1]:

$$\begin{aligned} g(n_1, n_2) &= d(n_1, n_2) * f(n_1, n_2) + w(n_1, n_2) \\ &= \sum_{k_1=0}^{N-1} \sum_{k_2=0}^{M-1} d(k_1, k_2) f(n_1 - k_1, n_2 - k_2) + w(n_1, n_2). \end{aligned} \quad (1)$$

Here $w(n_1, n_2)$ is the noise that corrupts the blurred image. Clearly the objective of image restoration is to make an estimate $\hat{f}(n_1, n_2)$ of the ideal image $f(n_1, n_2)$, given only the degraded image $g(n_1, n_2)$, the blurring function $d(n_1, n_2)$ and some information about the statistical properties of the ideal image and the noise.

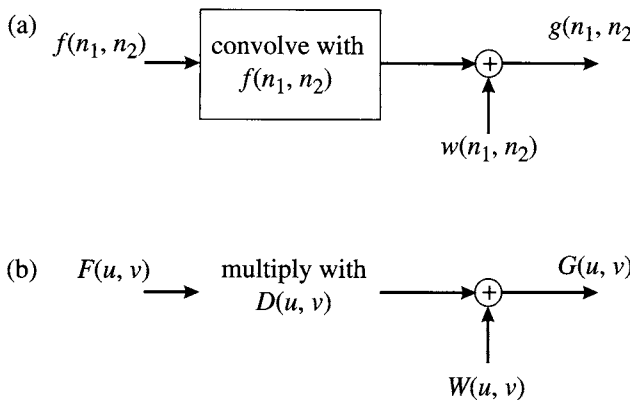


FIGURE 1 (a) Image formation model in the spatial domain. (b) Image formation model in the Fourier domain.

An alternative way of describing (1) is through its spectral equivalence. By applying discrete Fourier transforms to (1), we obtain the following representation (see also Fig. 1(b)):

$$G(u, v) = D(u, v)F(u, v) + W(u, v) \quad (2)$$

where (u, v) are the spatial frequency coordinates, and capitals represent Fourier transforms. Either (1) or (2) can be used for developing restoration algorithms. In practice the spectral representation is more often used since it leads to efficient implementations of restoration filters in the (discrete) Fourier domain.

In (1) and (2), the noise $w(n_1, n_2)$ is modeled as an additive term. Typically the noise is considered to have a zero mean and to be white, i.e., spatially uncorrelated. In statistical terms this can be expressed as follows [15]:

$$E[w(n_1, n_2)] \approx \frac{1}{NM} \sum_{k_1=0}^{N-1} \sum_{k_2=0}^{M-1} w(k_1, k_2) = 0 \quad (3a)$$

$$\begin{aligned} R_w(k_1, k_2) &= E[w(n_1, n_2)w(n_1 - k_1, n_2 - k_2)] \\ &\approx \frac{1}{NM} \sum_{n_1=0}^{N-1} \sum_{n_2=0}^{M-1} w(n_1, n_2)w(n_1 - k_1, n_2 - k_2) \\ &= \begin{cases} \sigma_w^2 & \text{if } k_1 = k_2 = 0 \\ 0 & \text{otherwise} \end{cases}. \end{aligned} \quad (3b)$$

Here σ_w^2 is the variance or power of the noise and $E[\cdot]$ refers to the expected value operator. The approximate equality indicates that on the average equation (3) should hold, but that for a given image (3) holds only approximately as a result of replacing the expectation by a pixel-wise summation over the image. Sometimes the noise is assumed to have a Gaussian probability density function, but for none of the restoration algorithms described in this chapter is this a necessary condition.

In general the noise $w(n_1, n_2)$ may not be independent of the ideal image $f(n_1, n_2)$. This may happen for instance if the image formation process contains non-linear components, or if the noise is multiplicative instead of additive. Unfortunately, this dependency is often difficult to model or to estimate. Therefore, noise and ideal image are usually assumed to be orthogonal, which is — in this case — equivalent to being uncorrelated because the noise has zero-mean. In statistical terms expressed, the following condition holds:

$$\begin{aligned} R_{fw}(k_1, k_2) &= E[f(n_1, n_2)w(n_1 - k_1, n_2 - k_2)] \\ &\approx \frac{1}{NM} \sum_{n_1=0}^{N-1} \sum_{n_2=0}^{M-1} f(n_1, n_2)w(n_1 - k_1, n_2 - k_2) = 0. \end{aligned} \quad (4)$$

The above models (1)–(4) form the foundations for the class of linear spatially invariant image restoration and accompanying blur identification algorithms. In particular these models apply to monochromatic images. For color images, two approaches can be taken. In the first place one can extend equations (1)–(4) to incorporate multiple color components. In many practical cases of interest this is indeed the proper way of modeling the problem of color image restoration since the degradations of the different color components (such as the tri-stimulus signals red-green-blue, luminance-hue-saturation, or luminance-chrominance) are not independent. This leads to a class of algorithms known as “multi-frame filters” [5, 9]. A second, more pragmatic, way of dealing with color images is to assume that the noises and blurs in each of the color components are independent. The restoration of the color components can then be carried out independently as well, meaning that each color component is simply regarded as a monochromatic image by itself, forgetting about the other color components. Though obviously this model might be in error, acceptable results have been achieved in this way.

The outline of this chapter is as follows. In Section 2, we first describe several important models for linear blurs, namely motion blur, out-of-focus blur, and blur due to atmospheric turbulence. In the Section 3, three classes of restoration algorithms are introduced and described in detail, namely the inverse filter, the Wiener and constrained least-squares filter, and the iterative restoration filters. In Section 4, two basic approaches to blur identification will be described.

2 Blur Models

The blurring of images is modeled in (1) as the convolution of an ideal image with a 2D point-spread function (PSF) $d(n_1, n_2)$. The interpretation of (1) is that if the ideal image $f(n_1, n_2)$ would consist of a single intensity point or point source, this point would be recorded as a spread-out intensity pattern¹ $d(n_1, n_2)$, hence the name *point-spread* function.

It is worth noticing that point-spread functions in this chapter are not a function of the spatial location under consideration, i.e., they are spatially invariant. Essentially this means that the image is blurred in exactly the same way at every spatial location. Point-spread functions that do not follow this assumption are, for instance, due to rotational blurs (turning wheels) or local blurs (a person out of focus while the background is in focus). The modeling, restoration and identification of images degraded by spatially varying blurs is outside the scope of this chapter, and is actually still a largely unsolved problem.

In most cases the blurring of images is a spatially continuous process. Since identification and restoration algorithms are always based on spatially discrete images, we present

¹Ignoring the noise for a moment.

the blur models in their continuous forms, followed by their discrete (sampled) counterparts. We assume that the sampling rate of the images has been chosen high enough to minimize the (aliasing) errors involved in going from the continuous to discrete models.

The spatially continuous PSF $d(x, y)$ of any blur satisfies three constraints, namely:

- $d(x, y)$ takes on non-negative values only, because of the physics of the underlying image formation process,
- when dealing with real-valued images the point-spread function $d(x, y)$ is real-valued too,
- the imperfections in the image formation process are modeled as passive operations on the data, i.e., no “energy” is absorbed or generated. Consequently, for spatially continuous blurs the PSF is constrained to satisfy

$$\int_{-\infty}^{\infty} \int_{-\infty}^{\infty} d(x, y) dx dy = 1, \quad (5a)$$

and for spatially discrete blurs:

$$\sum_{n_1=0}^{N-1} \sum_{n_2=0}^{M-1} d(n_1, n_2) = 1. \quad (5b)$$

In the following we will present four common point-spread functions, which are encountered regularly in practical situations of interest.

2.1 No Blur

In case the recorded image is imaged perfectly, no blur will be apparent in the discrete image. The spatially continuous PSF can then be modeled as a Dirac delta function:

$$d(x, y) = \delta(x, y) \quad (6a)$$

and the spatially discrete PSF as a unit pulse:

$$d(n_1, n_2) = \delta(n_1, n_2) = \begin{cases} 1 & \text{if } n_1 = n_2 = 0 \\ 0 & \text{elsewhere} \end{cases}. \quad (6b)$$

Theoretically (6a) can never be satisfied. However, as long as the amount of “spreading” in the continuous image is smaller than the sampling grid applied to obtain the discrete image, equation (6b) will be arrived at.

2.2 Linear Motion Blur

Many types of motion blur can be distinguished all of which are due to relative motion between the recording device and the scene. This can be in the form of a translation, a rotation, a sudden change of scale, or some combinations of these.

Here only the important case of a global translation will be considered.

When the scene to be recorded translates relative to the camera at a constant velocity v_{relative} under an angle of ϕ radians with the horizontal axis during the exposure interval $[0, t_{\text{exposure}}]$, the distortion is one-dimensional. Defining the “length of motion” by $L = v_{\text{relative}} t_{\text{exposure}}$, the PSF is given by:

$$d(x, y; L, \phi) = \begin{cases} \frac{1}{L} & \text{if } \sqrt{x^2 + y^2} \leq \frac{L}{2} \text{ and } \frac{x}{y} = -\tan \phi \\ 0 & \text{elsewhere} \end{cases}. \quad (7a)$$

The discrete version of (7a) is not easily captured in a closed form expression in general. For the special case that $\phi = 0$, an appropriate approximation is:

$$\begin{aligned} d(n_1, n_2; L) &= \begin{cases} \frac{1}{L} & \text{if } n_1 = 0, |n_2| \leq \left\lfloor \frac{L-1}{2} \right\rfloor \\ \frac{1}{2L} \left\{ (L-1) - 2 \left\lfloor \frac{L-1}{2} \right\rfloor \right\} & \text{if } n_1 = 0, |n_2| = \left\lceil \frac{L-1}{2} \right\rceil \\ 0 & \text{elsewhere} \end{cases} \\ &\quad (7b) \end{aligned}$$

Figure 2(a) shows the modulus of the Fourier transform of the PSF of motion blur with $L = 7.5$ and $\phi = 0$. This figure illustrates that the blur is effectively a horizontal low-pass filtering operation and that the blur has spectral zeros along characteristic lines. The interline spacing of these characteristic zero pattern is (for the case that $N = M$) approximately equal to N/L . Figure 2(b) shows the modulus of the Fourier transform for the case of $L = 7.5$ and $\phi = \pi/4$.

2.3 Uniform Out-of-Focus Blur

When a camera images a 3D scene onto a 2D imaging plane, some parts of the scene are in focus while other parts are not. If the aperture of the camera is circular, the image of any

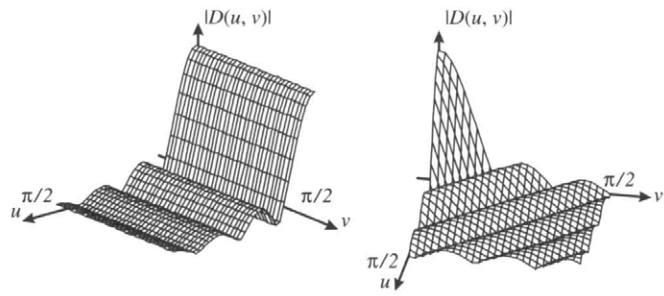


FIGURE 2 PSF of motion blur in the Fourier domain, showing $|D(u, v)|$, for (a) $L = 7.5$ and $\phi = 0$; (b) $L = 7.5$ and $\phi = \pi/4$.

point source is a small disk, known as the circle of confusion (COC). The degree of defocus (diameter of the COC) depends on the focal length and the aperture number of the lens, and the distance between camera and object. An accurate model not only describes the diameter of the COC, but also the intensity distribution within the COC. However, if the degree of defocusing is large relative to the wavelengths considered, a geometrical approach can be followed resulting in a uniform intensity distribution within the COC. The spatially continuous PSF of this uniform out-of-focus blur with radius R is given by:

$$d(x, y; R) = \begin{cases} \frac{1}{\pi R^2} & \text{if } \sqrt{x^2 + y^2} \leq R^2 \\ 0 & \text{elsewhere} \end{cases}. \quad (8a)$$

Also for this PSF the discrete version $d(n_1, n_2)$ is not easily arrived at. A coarse approximation is the following spatially discrete PSF:

$$d(n_1, n_2; R) = \begin{cases} \frac{1}{C} & \text{if } \sqrt{n_1^2 + n_2^2} \leq R^2 \\ 0 & \text{elsewhere} \end{cases} \quad (8b)$$

where C is a constant that must be chosen so that (5b) is satisfied. The approximation (8b) is incorrect for the fringe elements of the point-spread function. A more accurate model for the fringe elements would involve the integration of the area covered by the spatially continuous PSF, as illustrated in Fig. 3. Figure 3(a) shows the fringe elements that need to be calculated by integration. Figure 3(b) shows the modulus of the Fourier transform of the PSF for $R = 2.5$. Again a low pass behavior can be observed (in this case both horizontally and vertically), as well as a characteristic pattern of spectral zeros.

2.4 Atmospheric Turbulence Blur

Atmospheric turbulence is a severe limitation in remote sensing. Although the blur introduced by atmospheric

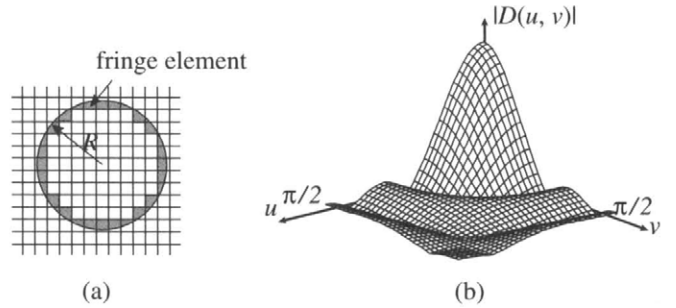


FIGURE 3 (a) Fringe elements of discrete out-of-focus blur that are calculated by integration; (b) PSF in the Fourier domain, showing $|D(u, v)|$, for $R = 2.5$.

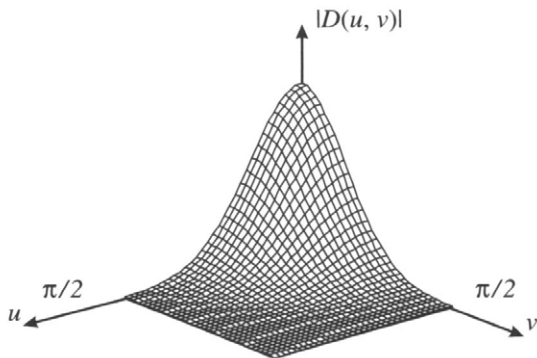


FIGURE 4 Gaussian PSF in the Fourier domain ($\sigma_G = 1.2$).

turbulence depends on a variety of factors (such as temperature, wind speed, exposure time), for long-term exposures the point-spread function can be described reasonably well by a Gaussian function:

$$d(x, y; \sigma_G) = C \exp\left(-\frac{x^2 + y^2}{2\sigma_G^2}\right). \quad (9a)$$

Here σ_G determines the amount of spread of the blur, and the constant C is to be chosen so that (5a) is satisfied. Since (9a) constitutes a PSF that is separable in a horizontal and a vertical component, the discrete version of (9a) is usually obtained by first computing a 1D discrete Gaussian PSF $\tilde{d}(n)$. This 1D PSF is found by a numeric discretization of the continuous PSF. For each PSF element $\tilde{d}(n)$ the 1D continuous PSF is integrated over the area covered by the 1D sampling grid, namely $[n - \frac{1}{2}, n + \frac{1}{2}]$:

$$\tilde{d}(n; \sigma_G) = C \int_{n-\frac{1}{2}}^{n+\frac{1}{2}} \exp\left(-\frac{x^2}{2\sigma_G^2}\right) dx. \quad (9b)$$

Since the spatially continuous PSF does not have a finite support, it has to be truncated properly. The spatially discrete approximation of (9a) is then given by:

$$d(n_1, n_2; \sigma_G) = \tilde{d}(n_1; \sigma_G) \tilde{d}(n_2; \sigma_G). \quad (9c)$$

Figure 4 shows this PSF in the spectral domain ($\sigma_G = 1.2$). Observe that Gaussian blurs do not have exact spectral zeros.

3 Image Restoration Algorithms

In this section we will assume that the PSF of the blur is satisfactorily known. A number of methods will be introduced for removing the blur from the recorded image $g(n_1, n_2)$ using a linear filter. Once the point-spread function of the linear

restoration filter, denoted by $h(n_1, n_2)$, has been designed, the restored image is given by

$$\begin{aligned} \hat{f}(n_1, n_2) &= h(n_1, n_2) * g(n_1, n_2) \\ &= \sum_{k_1=0}^{N-1} \sum_{k_2=0}^{M-1} h(k_1, k_2) g(n_1 - k_1, n_2 - k_2) \end{aligned} \quad (10a)$$

or in the spectral domain by

$$\hat{F}(u, v) = H(u, v)G(u, v). \quad (10b)$$

The objective of this section is to design appropriate restoration filters $h(n_1, n_2)$ or $H(u, v)$ for use in (10).

In image restoration the improvement in quality of the restored image over the recorded blurred one is measured by the signal-to-noise ratio improvement. The signal-to-noise ratio of the recorded (blurred and noisy) image is defined as follows in decibels:

$$\begin{aligned} \text{SNR}_g &= 10 \log_{10} \left(\frac{\text{variance of the ideal image } f(n_1, n_2)}{\text{variance of the difference image } g(n_1, n_2) - f(n_1, n_2)} \right) (\text{dB}). \end{aligned} \quad (11a)$$

The signal-to-noise ratio of the restored image is similarly defined as:

$$\begin{aligned} \text{SNR}_{\hat{f}} &= 10 \log_{10} \left(\frac{\text{variance of the ideal image } f(n_1, n_2)}{\text{variance of the difference image } \hat{f}(n_1, n_2) - f(n_1, n_2)} \right) (\text{dB}). \end{aligned} \quad (11b)$$

Then, the improvement in signal-to-noise ratio is given by

$$\begin{aligned} \Delta \text{SNR} &= \text{SNR}_{\hat{f}} - \text{SNR}_g \\ &= 10 \log_{10} \left(\frac{\text{variance of the difference image } g(n_1, n_2) - f(n_1, n_2)}{\text{variance of the difference image } \hat{f}(n_1, n_2) - f(n_1, n_2)} \right) (\text{dB}). \end{aligned} \quad (11c)$$

The improvement in SNR is basically a measure that expresses the reduction of disagreement with the ideal image when comparing the distorted and restored image. Note that all of the above signal-to-noise measures can only be computed in case the ideal image $f(n_1, n_2)$ is available, i.e., in an experimental setup or in a design phase of the restoration algorithm. When applying restoration filters to real images of which the ideal image is not available, often only the visual judgment of the restored image can be relied upon. For this reason it

is desirable for a restoration filter to be somewhat “tunable” to the liking of the user.

3.1 Inverse Filter

An inverse filter is a linear filter whose point-spread function $h_{\text{inv}}(n_1, n_2)$ is the inverse of the blurring function $d(n_1, n_2)$, in the sense that:

$$h_{\text{inv}}(n_1, n_2) * d(n_1, n_2) = \sum_{k_1=0}^{N-1} \sum_{k_2=0}^{M-1} h_{\text{inv}}(k_1, k_2) d(n_1 - k_1, n_2 - k_2) = \delta(n_1, n_2). \quad (12)$$

When formulated as in (12), inverse filters seem difficult to design. However, the spectral counterpart of (12) immediately shows the solution to this design problem [1]:

$$H_{\text{inv}}(u, v)D(u, v) = 1 \Rightarrow H_{\text{inv}}(u, v) = \frac{1}{D(u, v)}. \quad (13)$$

The advantage of the *inverse filter* is that it requires only the blur PSF as *a priori* knowledge, and that it allows for perfect restoration in the case that noise is absent, as can easily be seen by substituting (13) into (10b):

$$\begin{aligned} \hat{F}_{\text{inv}}(u, v) &= H_{\text{inv}}(u, v)G(u, v) = \frac{1}{D(u, v)}(D(u, v)F(u, v) + W(u, v)) \\ &= F(u, v) + \frac{W(u, v)}{D(u, v)}. \end{aligned} \quad (14)$$

If the noise is absent, the second term in (14) disappears so that the restored image is identical to the ideal image. Unfortunately, several problems exist with (14). In the first place the inverse filter may not exist because $D(u, v)$ is zero at selected frequencies (u, v) . This happens for both the linear motion blur and the out-of-focus blur described in the previous section. Secondly, even if the blurring function's spectral representation $D(u, v)$ does not actually go to zero but becomes small, the second term in (14) — known as the inverse filtered noise — will become very large. Inverse filtered images are therefore often dominated by excessively amplified noise.²

Figure 5(a) shows an image degraded by out-of-focus blur ($R=2.5$) and noise. The inverse filtered version is shown in Fig. 5(b), clearly illustrating its uselessness. The Fourier transforms of the restored image and of $H_{\text{inv}}(u, v)$ are shown in Figs. 5(c) and (d), respectively, demonstrating that indeed the spectral zeros of the PSF cause problems.

²In literature, this effect is commonly referred to as the ill-conditionedness or ill-posedness of the restoration problem.

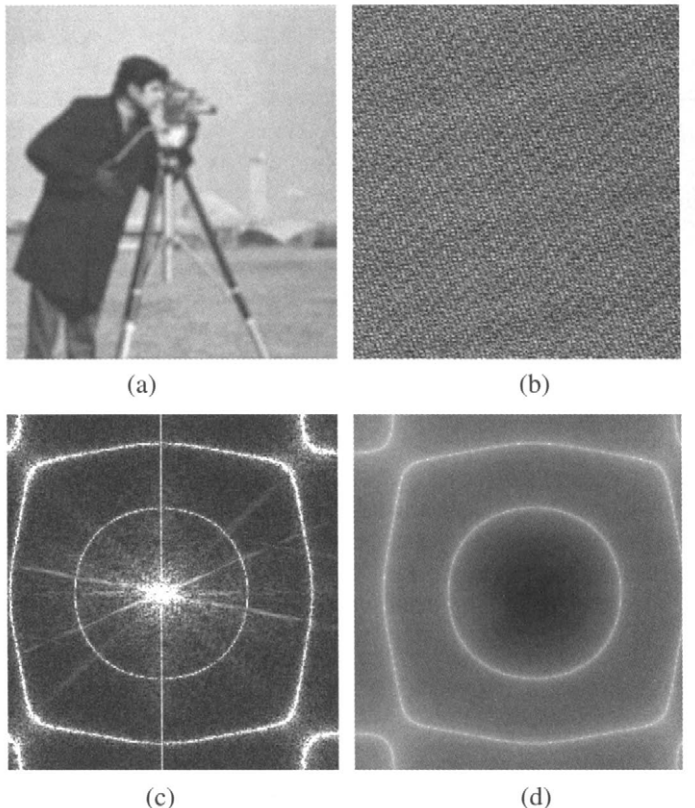


FIGURE 5 (a) Image out-of-focus with $\text{SNR}_g = 10.3$ dB (noise variance = 0.35); (b) inverse filtered image; (c) magnitude of the Fourier transform of the restored image. The DC component lies in the center of the image. The oriented white lines are spectral components of the image with large energy; (d) magnitude of the Fourier transform of the inverse filter response.

3.2 Least-Squares Filters

To overcome the noise sensitivity of the inverse filter, a number of restoration filters have been developed that are collectively called least-squares filters. We describe the two most commonly used filters from this collection, namely the Wiener filter and the constrained least-squares filter.

The Wiener filter is a linear spatially invariant filter of the form (10a), in which the point-spread function $h(n_1, n_2)$ is chosen such that it minimizes the mean-squared error (MSE) between the ideal and the restored image. This criterion attempts to make the difference between the ideal image and the restored one — i.e., the remaining restoration error — as small as possible *on the average*:

$$\begin{aligned} \text{MSE} &= E \left[(f(n_1, n_2) - \hat{f}(n_1, n_2))^2 \right] \\ &\approx \frac{1}{NM} \sum_{n_1=0}^{N-1} \sum_{n_2=0}^{M-1} (f(n_1, n_2) - \hat{f}(n_1, n_2))^2 \end{aligned} \quad (15)$$

where $\hat{f}(n_1, n_2)$ is given by (10a). The solution of this minimization problem is known as the *Wiener filter*, and is easiest defined in the spectral domain:

$$H_{\text{wiener}}(u, v) = \frac{D^*(u, v)}{D^*(u, v)D(u, v) + \frac{S_w(u, v)}{S_f(u, v)}}. \quad (16)$$

Here $D^*(u, v)$ is the complex conjugate of $D(u, v)$, and $S_f(u, v)$ and $S_w(u, v)$ are the power spectrum of the ideal image and the noise, respectively. The power spectrum is a measure for the average signal power per spatial frequency (u, v) carried by the image. In the noiseless case we have $S_w(u, v) = 0$, so that the Wiener filter approximates the inverse filter:

$$H_{\text{wiener}}(u, v)|_{S_w(u, v) \rightarrow 0} = \begin{cases} \frac{1}{D(u, v)} & \text{for } D(u, v) \neq 0 \\ 0 & \text{for } D(u, v) = 0 \end{cases}. \quad (17)$$

For the more typical situation where the recorded image is noisy, the Wiener filter trades-off the restoration by inverse filtering and suppression of noise for those frequencies where $D(u, v) \rightarrow 0$. The important factors in this trade-off are the power spectra of the ideal image and the noise. For spatial frequencies where $S_w(u, v) \ll S_f(u, v)$, the Wiener filter approaches the inverse filter, while for spatial frequencies where $S_w(u, v) \gg S_f(u, v)$ the Wiener filter acts as a frequency rejection filter, i.e., $H_{\text{wiener}}(u, v) \rightarrow 0$.

If we assume that the noise is uncorrelated (white noise), its power spectrum is determined by the noise variance only:

$$S_w(u, v) = \sigma_w^2 \quad \text{for all } (u, v). \quad (18)$$

Thus, it is sufficient to estimate the noise variance from the recorded image to get an estimate of $S_w(u, v)$. The estimation of the noise variance can also be left to the user of the Wiener filter as if it were a tunable parameter. Small values of σ_w^2 will yield a result close to the inverse filter, while large values will over-smooth the restored image.

The estimation of $S_f(u, v)$ is somewhat more problematic since the ideal image is obviously not available. There are three possible approaches to take. In the first place, one can replace $S_f(u, v)$ by an estimate of the power spectrum of the blurred image and compensate for the variance of the noise σ_w^2 :

$$S_f(u, v) \approx S_g(u, v) - \sigma_w^2 \approx \frac{1}{NM} G^*(u, v)G(u, v) - \sigma_w^2. \quad (19)$$

The above used estimator for the power spectrum $S_g(u, v)$ of $g(n_1, n_2)$ is known as the periodogram. This estimator requires little *a priori* knowledge, but it is known to have

several shortcomings. More elaborate estimators for the power spectrum exist, but these require much more *a priori* knowledge.

A second approach is to estimate the power spectrum $S_f(u, v)$ from a set of representative images. These representative images are to be taken from a collection of images that have a content “similar” to the image that needs to be restored. Of course, one still needs an appropriate estimator to obtain the power spectrum from the set of representative images.

The third and final approach is to use a statistical model for the ideal image. Often these models incorporate parameters that can be tuned to the actual image being used. A widely used image model — not only popular in image restoration but also in image compression — is the following 2D causal auto-regressive model [8]:

$$\begin{aligned} f(n_1, n_2) = & a_{0,1}f(n_1, n_2 - 1) + a_{1,1}f(n_1 - 1, n_2 - 1) \\ & + a_{1,0}f(n_1 - 1, n_2) + v(n_1, n_2). \end{aligned} \quad (20a)$$

In this model the intensities at the spatial location (n_1, n_2) are described as the sum of weighted intensities at neighboring spatial locations and a small unpredictable component $v(n_1, n_2)$. The unpredictable component is often modeled as white noise with variance σ_v^2 . Table 1 gives numeric examples for mean-square error estimates of the *prediction coefficients* $a_{i,j}$ for some images. For the mean-square error estimation of these parameters first the 2D autocorrelation function has been estimated, which is then used in the Yule-Walker equations [8]. Once the model parameters for (20a) have been chosen, the power spectrum can be calculated to be equal to

$$S_f(u, v) = \frac{\sigma_v^2}{|1 - a_{0,1}e^{-ju} - a_{1,1}e^{-ju-jv} - a_{1,0}e^{-jv}|^2}. \quad (20b)$$

The trade-off between noise smoothing and deblurring that is made by the Wiener filter is illustrated in Fig. 6. Going from 6(a) to 6(c) the variance of the noise in the degraded image, i.e., σ_w^2 , has been estimated too large, optimally, and

TABLE 1 Prediction coefficients and variance of $v(n_1, n_2)$ for four images, computed in the mean-square error optimal sense by the Yule-Walker equations.

	$a_{0,1}$	$a_{1,1}$	$a_{1,0}$	σ_v^2
Cameraman	0.709	-0.467	0.739	231.8
Lena	0.511	-0.343	0.812	132.7
Trevor White	0.759	-0.525	0.764	33.0
White noise	-0.008	-0.003	-0.002	5470.1

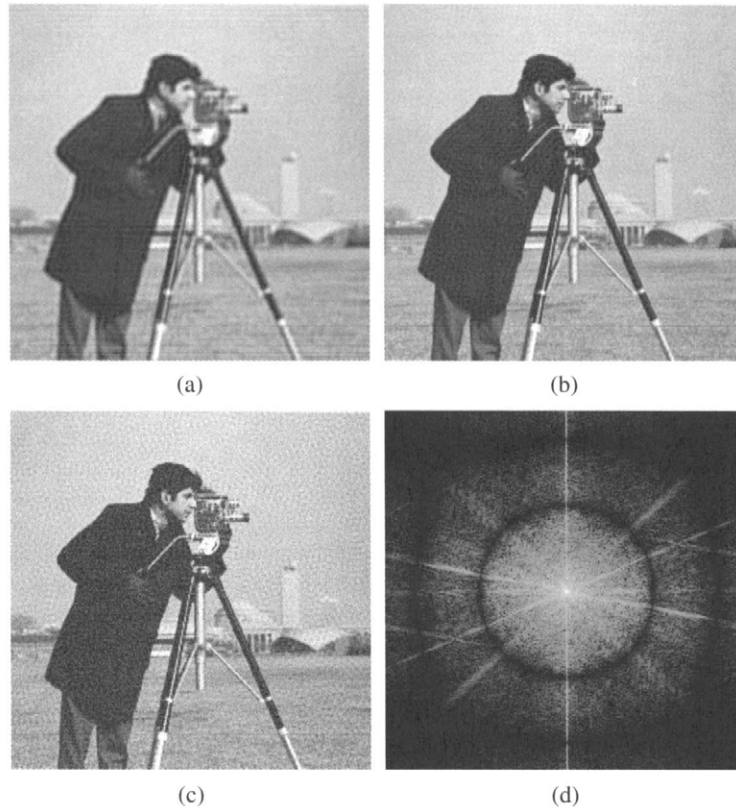


FIGURE 6 (a) Wiener restoration of image in Fig. 5(a) with assumed noise variance equal to 35.0 ($\Delta \text{SNR} = 3.7 \text{ dB}$); (b) restoration using the correct noise variance of 0.35 ($\Delta \text{SNR} = 8.8 \text{ dB}$); (c) restoration assuming the noise variance is 0.0035 ($\Delta \text{SNR} = 1.1 \text{ dB}$); (d) magnitude of the Fourier transform of the restored image in Fig. 6b.

too small, respectively. The visual differences, as well as the differences in improvement in SNR (ΔSNR) are substantial. The power spectrum of the original image has been calculated from the model (20a). From the results it is clear that the excessive noise amplification of the earlier example is no longer present because of the masking of the spectral zeros (see Fig. 6(d)). Typical artifacts of the Wiener restoration — and actually of most restoration filters — are the residual blur in the image and the “ringing” or “halo” artifacts present near edges in the restored image.

The *constrained least-squares filter* [7] is another approach for overcoming some of the difficulties of the inverse filter (excessive noise amplification) and of the Wiener filter (estimation of the power spectrum of the ideal image), while still retaining the simplicity of a spatially invariant linear filter. If the restoration is a good one, the blurred version of the restored image should be approximately equal to the recorded distorted image. That is:

$$d(n_1, n_2) * \hat{f}(n_1, n_2) \approx g(n_1, n_2). \quad (21)$$

With the inverse filter the approximation is made exact, which leads to problems because a match is made to noisy data.

A more reasonable expectation for the restored image is that it satisfies:

$$\begin{aligned} & \|g(n_1, n_2) - d(n_1, n_2) * \hat{f}(n_1, n_2)\|^2 \\ &= \frac{1}{NM} \sum_{k_1=0}^{N-1} \sum_{k_2=0}^{M-1} (g(k_1, k_2) - d(k_1, k_2) * \hat{f}(k_1, k_2))^2 \approx \sigma_w^2. \end{aligned} \quad (22)$$

There are potentially many solutions that satisfy the above relation. A second criterion must be used to choose among them. A common criterion, acknowledging the fact that the inverse filter tends to amplify the noise $w(n_1, n_2)$, is to select the solution that is as “smooth” as possible. If we let $c(n_1, n_2)$ represent the point-spread function of a 2D high-pass filter, then among the solutions satisfying (22) the solution is chosen that minimizes

$$\begin{aligned} \Omega(\hat{f}(n_1, n_2)) &= \|c(n_1, n_2) * \hat{f}(n_1, n_2)\|^2 \\ &= \frac{1}{NM} \sum_{k_1=0}^{N-1} \sum_{k_2=0}^{M-1} (c(k_1, k_2) * \hat{f}(k_1, k_2))^2. \end{aligned} \quad (23)$$

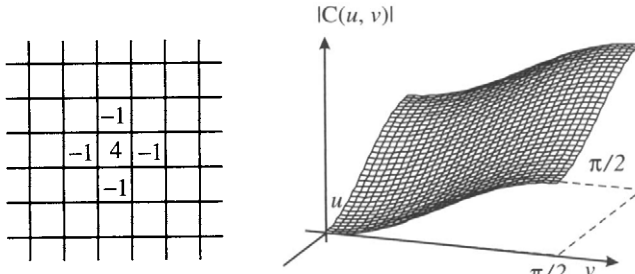


FIGURE 7 Two-dimensional discrete approximation of the second derivative operation. (a) PSF $c(n_1, n_2)$; (b) spectral representation.

The interpretation of $\Omega(\hat{f}(n_1, n_2))$ is that it gives a measure for the high frequency content of the restored image. Minimizing this measure subject to the constraint (22) will give a solution that is both within the collection of potential solutions of (22) and has as little high-frequency content as possible at the same time. A typical choice for $c(n_1, n_2)$ is the discrete approximation of the second derivative shown in Fig. 7, also known as the 2D Laplacian operator. For more details on the subject of discrete derivative operators, refer to Chapter 4.10 of this *Handbook*.

The solution to the above minimization problem is the constrained least-squares filter $H_{cls}(u, v)$ that is easiest formulated in the discrete Fourier domain:

$$H_{cls}(u, v) = \frac{D^*(u, v)}{D^*(u, v)D(u, v) + \alpha C^*(u, v)C(u, v)}. \quad (24)$$

Here α is a tuning or *regularization* parameter that should be chosen such that (22) is satisfied. Though analytical approaches exist to estimate α [9], the regularization parameter is usually considered user tunable.

It should be noted that although their motivations are quite different, the formulation of the Wiener filter (16) and

constrained least-squares filter (24) are quite similar. Indeed these filters perform equally well, and they behave similarly in the case that the variance of the noise, σ_w^2 , approaches zero. Figure 8 shows restoration results obtained by the constrained least-squares filter using three different values of α . A final remark about $\Omega(\hat{f}(n_1, n_2))$ is that the inclusion of this criterion is strongly related to using an image model. A vast amount of literature exists on the usage of more complicated image models, especially the ones inspired by 2D auto-regressive processes [17] and the Markov random field theory [6].

3.3 Iterative Filters

The filters formulated in the previous two sections are usually implemented in the Fourier domain using Eq. (10b). Compared to the spatial domain implementation in Eq. (10a), the direct convolution with the 2D point-spread function $h(n_1, n_2)$ can be avoided. This is a great advantage because $h(n_1, n_2)$ has a very large support, and typically contains NM non-zero filter coefficients even if the PSF of the blur has a small support that contains only a few non-zero coefficients. There are, however, two situations in which spatial domain convolutions are preferred over the Fourier domain implementation, namely:

- in situations where the dimensions of the image to be restored are very large,
- in cases where additional knowledge is available about the restored image, especially if this knowledge cannot be cast in the form of Eq. (23). An example is the *a priori* knowledge that image intensities are always positive. Both in the Wiener and the constrained least-squares filter the restored image may come out with negative intensities, simply because negative restored signal values are not explicitly prohibited in the design of the restoration filter.

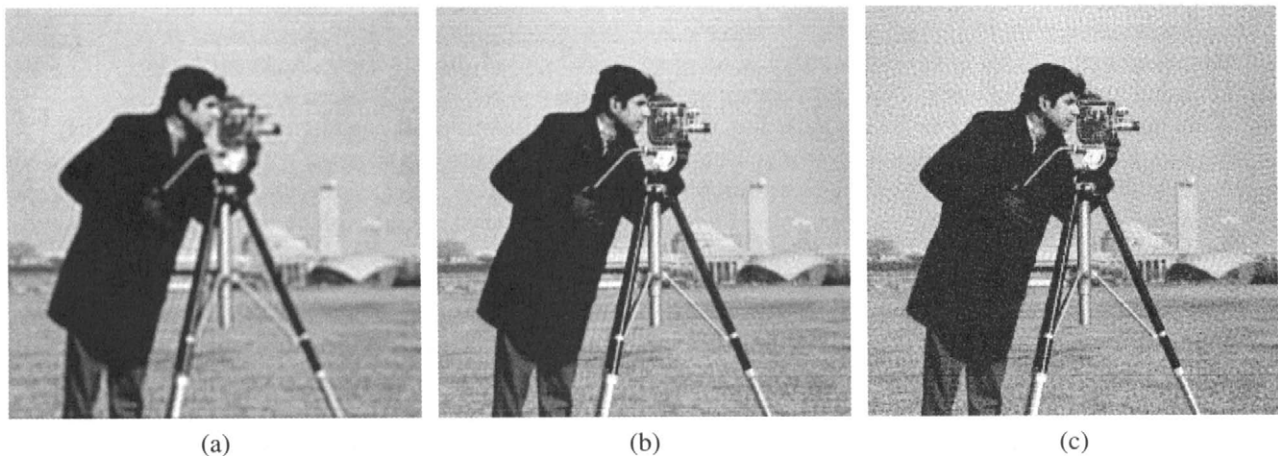


FIGURE 8 (a) Constrained least-squares restoration of image in Fig. 5(a) with $\alpha = 2 \times 10^{-2}$ ($\Delta SNR = 1.7$ dB); (b) $\alpha = 2 \times 10^{-4}$ ($\Delta SNR = 6.9$ dB); (c) $\alpha = 2 \times 10^{-6}$ ($\Delta SNR = 0.8$ dB).

Iterative restoration filters provide a means to handle the above situations elegantly [3, 10, 14]. The basic form of iterative restoration filters is the one that iteratively approaches the solution of the inverse filter, and is given by the following spatial domain iteration:

$$\hat{f}_{i+1}(n_1, n_2) = \hat{f}_i(n_1, n_2) + \beta(g(n_1, n_2) - d(n_1, n_2) * \hat{f}_i(n_1, n_2)). \quad (25)$$

Here $\hat{f}_i(n_1, n_2)$ is the restoration result after i iterations. Usually in the first iteration $\hat{f}_0(n_1, n_2)$ is chosen to be identical to zero or identical to $g(n_1, n_2)$. The iteration (25) has been independently discovered many times, and is referred to as the van Cittert, Bally, or Landweber iteration. As can be seen from (25), during the iterations the blurred version of the current restoration result $\hat{f}_i(n_1, n_2)$ is compared to the recorded image $g(n_1, n_2)$. The difference between the two is scaled and added to the current restoration result to give the next restoration result.

With iterative algorithms, there are two important concerns — does it converge and, if so, to what limiting solution? Analyzing (25) shows that convergence occurs if the convergence parameter β satisfies:

$$|1 - \beta D(u, v)| < 1 \quad \text{for all } (u, v). \quad (26a)$$

Using the fact that $|D(u, v)| \leq 1$, this condition simplifies to:

$$0 < \beta < 2 \quad \text{and} \quad D(u, v) > 0. \quad (26b)$$

If the number of iterations becomes very large, then $f_i(n_1, n_2)$ approaches the solution of the inverse filter:

$$\lim_{i \rightarrow \infty} \hat{f}_i(n_1, n_2) = h_{\text{inv}}(n_1, n_2) * g(n_1, n_2). \quad (27)$$

Figure 9 shows four restored images obtained by the iteration (25). Clearly as the iteration progresses, the restored image is dominated more and more by inverse filtered noise.

The iterative scheme (25) has several advantages and disadvantages that we will discuss next. The first advantage is that (25) does not require the convolution of images with 2D PSFs containing many coefficients. The only convolution is that of the restored image with the PSF of the blur, which has relatively few coefficients.

The second advantage is that no Fourier transforms are required, making (25) applicable to images of arbitrary size. The third advantage is that although the iteration produces the inverse filtered image as a result if the iteration is continued indefinitely, the iteration can be terminated whenever an acceptable restoration result has been achieved. Starting off with a blurred image, the iteration progressively deblurs the image. At the same time the noise will be amplified more and more as the iteration continues. It is now usually left to the

user to trade-off the degree of restoration against the noise amplification, and to stop the iteration when an acceptable partially deblurred result has been achieved.

The fourth advantage is that the basic form (25) can be extended to include all types of *a priori* knowledge. First all knowledge is formulated in the form of projective operations on the image [4]. After applying a projective operation the (restored) image satisfies the *a priori* knowledge reflected by that operator. For instance, the fact that image intensities are always positive can be formulated as the following projective operation P :

$$P[\hat{f}(n_1, n_2)] = \begin{cases} \hat{f}(n_1, n_2) & \text{if } \hat{f}(n_1, n_2) \geq 0 \\ 0 & \text{if } \hat{f}(n_1, n_2) < 0. \end{cases} \quad (28)$$

By including this projection P in the iteration, the final image after convergence of the iteration and all of the intermediate images will not contain negative intensities. The resulting iterative restoration algorithm now becomes

$$\hat{f}_{i+1}(n_1, n_2) = P[\hat{f}_i(n_1, n_2) + \beta(g(n_1, n_2) - d(n_1, n_2) * \hat{f}_i(n_1, n_2))]. \quad (29)$$

The requirements on β for convergence as well as the properties of the final image after convergence are difficult to analyze and fall outside the scope of this chapter. Practical values for β are typically around 1. Further, not all projections P can be used in the iteration (29), but only *convex* projections. A loose definition of a convex projection is the following. If two images $f^{(1)}(n_1, n_2)$ and $f^{(2)}(n_1, n_2)$ both satisfy the *a priori* information described by the projection P , then also the combined image

$$f^{(c)}(n_1, n_2) = \varepsilon f^{(1)}(n_1, n_2) + (1 - \varepsilon)f^{(2)}(n_1, n_2) \quad (30)$$

must satisfy this *a priori* information for all values of ε between 0 and 1.

A final advantage of iterative schemes is that they are easily extended for spatially variant restoration, i.e., restoration where either the PSF of the blur or the model of the ideal image (for instance the prediction coefficients in Eq. (20)) vary locally [9, 14].

On the negative side, the iterative scheme (25) has two disadvantages. In the first place the second requirement in Eq. (26b), namely that $D(u, v) > 0$, is not satisfied by many blurs, like motion blur and out-of-focus blur. This causes (25) to diverge for these types of blur. In the second place — unlike the Wiener and constrained least-squares filter — the basic scheme does not include any knowledge about the spectral behavior of the noise and the ideal image. Both disadvantages

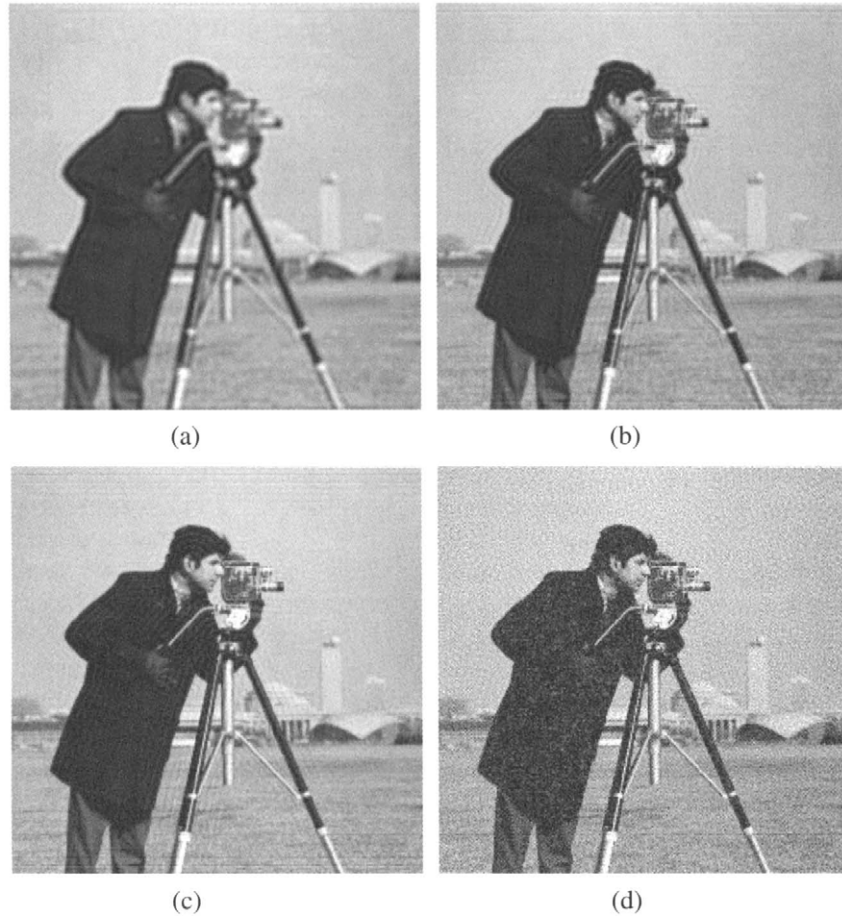


FIGURE 9 (a) Iterative restoration ($\beta = 1.9$) of the image in Fig. 5(a) after 10 iterations ($\Delta \text{SNR} = 1.6 \text{ dB}$), (b) after 100 iterations ($\Delta \text{SNR} = 5.0 \text{ dB}$), (c) after 500 iterations ($\Delta \text{SNR} = 6.6 \text{ dB}$), (d) after 5,000 iterations ($\Delta \text{SNR} = -2.6 \text{ dB}$).

can be corrected by modifying the basic iterative scheme as follows:

$$\begin{aligned}\hat{f}_{i+1}(n_1, n_2) &= (\delta(n_1, n_2) - \alpha\beta c(-n_1, -n_2) * c(n_1, n_2)) * \hat{f}_i(n_1, n_2) \\ &\quad + \beta d(-n_1, -n_2) * (g(n_1, n_2) - d(n_1, n_2) * \hat{f}_i(n_1, n_2)).\end{aligned}\quad (31)$$

Here α and $c(n_1, n_2)$ have the same meaning as in the constrained least-squares filter. Though the convergence requirements are more difficult to analyze, it is no longer necessary for $D(u, v)$ to be positive for all spatial frequencies. If the iteration is continued indefinitely, Eq. (31) will produce the constrained least-squares filtered image as result. In practice the iteration is terminated long before convergence. The precise termination point of the iterative scheme gives the user an additional degree of freedom over the direct implementation of the constrained least-squares filter. It is noteworthy that although (31) seems to involve many more convolutions than (25), a reorganization of terms is possible

revealing that many of those convolutions can be carried out once and off-line, and that only one convolution is needed per iteration:

$$\hat{f}_{i+1}(n_1, n_2) = g^d(n_1, n_2) + k(n_1, n_2) * \hat{f}_i(n_1, n_2) \quad (32a)$$

where the image $g^d(n_1, n_2)$ and the fixed convolution kernel $k(n_1, n_2)$ are given by

$$g^d(n_1, n_2) = \beta d(-n_1, -n_2) * g(n_1, n_2)$$

$$\begin{aligned}k(n_1, n_2) &= \delta(n_1, n_2) - \alpha\beta c(-n_1, -n_2) * c(n_1, n_2) \\ &\quad - \beta d(-n_1, -n_2) * d(n_1, n_2).\end{aligned}\quad (32b)$$

A second — and very significant — disadvantage of the iterations (25), (29)–(32) is the slow convergence. Per iteration the restored image $\hat{f}_i(n_1, n_2)$ changes only a little. Many iteration steps are therefore required before an acceptable point for termination of the iteration is reached. The reason is that the above iteration is essentially

a *steepest descent* optimization algorithms, which are known to be slow in convergence. It is possible to reformulate the iterations in the form of for instance a *conjugate gradient* algorithm, which exhibits a much higher convergence rate [14].

3.4 Boundary Value Problem

Images are always recorded by sensors of finite spatial extent. Since the convolution of the ideal image with the PSF of the blur extends beyond the borders of the observed degraded image, part of the information that is necessary to restore the border pixels is not available to the restoration process. This problem is known as the *boundary value problem*, and poses a severe problem to restoration filters. Although at first glance the boundary value problem seems to have a negligible effect because it affects only border pixels, this is not true at all. The point-spread function of the restoration filter has a very large support, typically as large as the image itself. Consequently, the effect of missing information at the borders of the image propagates throughout the image, in this way deteriorating the entire image. Figure 10(a) shows an example of a case where the missing information immediately outside the borders of the image is assumed to be equal to the mean value of the image, yielding dominant horizontal oscillation patterns due to the restoration of the horizontal motion blur.

Two solutions to the boundary value problem are used in practice. The choice depends on whether a spatial domain or a Fourier domain restoration filter is used. In a spatial domain filter missing image information outside the observed image can be estimated by extrapolating the available image data. In the extrapolation, a model for the observed image can be used, such as the one in equation (20), or more simple procedures can be used such as mirroring the image data

with respect to the image border. For instance, image data missing on the left-hand side of the image could be estimated as follows:

$$g(n_1, n_2 - k) = g(n_1, n_2 + k) \quad \text{for } k = 1, 2, 3, \dots \quad (33)$$

In case Fourier domain restoration filters are used, such as the ones in (16) or (24), one should realize that discrete Fourier transforms assume periodicity of the data to be transformed. Effectively in 2D Fourier transforms this means that the left and right-hand sides of the image are implicitly assumed to be connected, as well as the top and bottom part of the image. A consequence of this property — implicit to discrete Fourier transforms — is that missing image information at the left-hand side of the image will be taken from the right-hand side, and vice versa. Clearly in practice this image data may not correspond to the actual (but missing data) at all. A common way to fix this problem is to interpolate the image data at the borders such that the intensities at the left and right-hand side as well as the top and bottom of the image transit smoothly. Figure 10(b) shows what the restored image looks like if a border of five columns or rows is used for linearly interpolating between the image boundaries. Other forms of interpolation could be used, but in practice linear interpolation suffices. All restored images shown in this chapter have been preprocessed in this way to solve the boundary value problem.

4 Blur Identification Algorithms

In the previous section it was assumed that the point-spread function $d(n_1, n_2)$ of the blur was known. In many practical cases the actual restoration process has to be preceded by

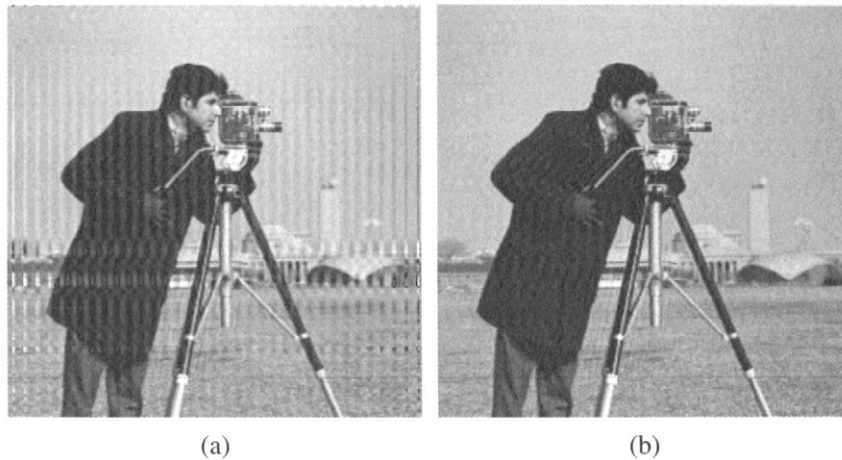


FIGURE 10 (a) Restored image illustrating the effect of the boundary value problem. The image was blurred by the motion blur shown in Fig. 2(a), and restored using the constrained least-squares filter; (b) preprocessed blurred image at its borders such that the boundary value problem is solved.

the identification of this point-spread function. If the camera misadjustment, object distances, object motion, and camera motion are known, we could — in theory — determine the PSF analytically. Such situations are, however, rare. A more common situation is that the blur is estimated from the observed image itself.

The blur identification procedure starts out by choosing a parametric model for the point-spread function. One category of parametric blur models has been given in Section II. As an example, if the blur were known to be due to motion, the blur identification procedure would estimate the length and direction of the motion.

A second category of parametric blur models is the one that describes the point-spread function $d(n_1, n_2)$ as a (small) set of coefficients within a given finite support. Within this support the value of the PSF coefficients needs to be estimated. For instance, if an initial analysis shows that the blur in the image resembles out-of-focus blur which, however, cannot be described parametrically by equation (8b), the blur PSF can be modeled as a square matrix of, say, size 3×3 , or 5×5 . The blur identification then requires the estimation of 9 or 25 PSF coefficients, respectively. This section describes the basics of the above two categories of blur estimation.

4.1 Spectral Blur Estimation

In Figs. 2 and 3 we have seen that two important classes of blurs, namely motion and out-of-focus blur, have spectral zeros. The structure of the zero-patterns characterizes the type and degree of blur within these two classes. Since the degraded image is described by (2), the spectral zeros of the PSF should also be visible in the Fourier transform $G(u, v)$, albeit that the zero-pattern might be slightly masked by the presence of the noise.

Figure 11 shows the modulus of the Fourier transform of two images, one subjected to motion blur and one to out-of-focus blur. From these images, the structure and

location of the zero-patterns can be estimated. In case the pattern contains dominant parallel lines of zeros, an estimate of the length and angle of motion can be made. In case dominant circular patterns occur, out-of-focus blur can be inferred and the degree of out-of-focus (the parameter R in equation (8)) can be estimated.

An alternative to the above method for identifying motion blur involves the computation of the 2D cepstrum of $g(n_1, n_2)$. The cepstrum is the inverse Fourier transform of the logarithm of $|G(u, v)|$. Thus:

$$\tilde{g}(n_1, n_2) = -F^{-1}\{\log |G(u, v)|\} \quad (34)$$

where F^{-1} is the inverse Fourier transform operator. If the noise can be neglected, $\tilde{g}(n_1, n_2)$ has a large spike at a distance L from the origin. Its position indicates the direction and extent of the motion blur. Figure 12 illustrates this effect for an image with the motion blur from Fig. 2(b).

4.2 Maximum Likelihood Blur Estimation

In case the point-spread function does not have characteristic spectral zeros or in case a parametric blur model such as motion or out-of-focus blur cannot be assumed, the individual coefficients of the point-spread function have to be estimated. To this end maximum likelihood estimation procedures for the unknown coefficients have been developed [9, 12, 13, 18]. Maximum likelihood estimation is a well-known technique for parameter estimation in situations where no stochastic knowledge is available about the parameters to be estimated [15].

Most maximum likelihood identification techniques begin by assuming that the ideal image can be described with the 2D auto-regressive model (20a). The parameters of this image model — that is, the prediction coefficients $a_{i,j}$ and the

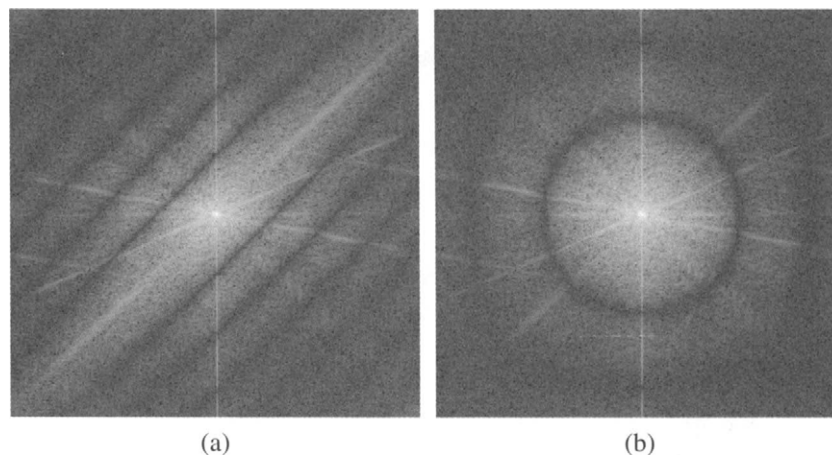


FIGURE 11 $|G(u, v)|$ of two blurred images.

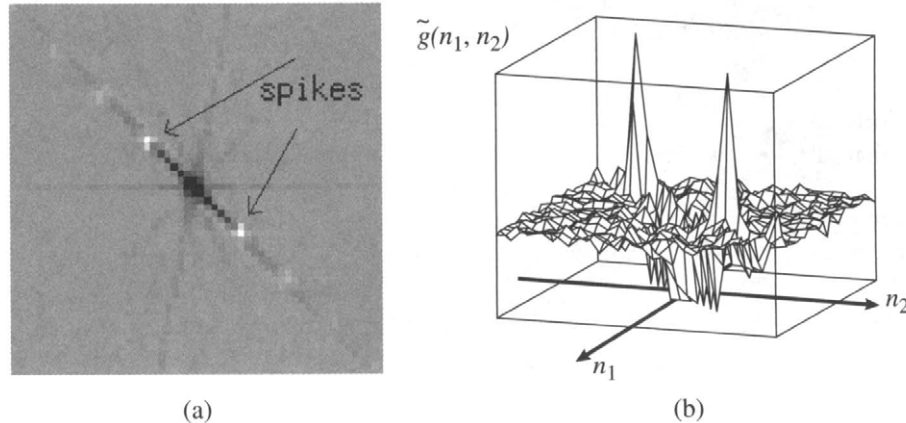


FIGURE 12 Cepstrum for motion blur from Fig. 2(c). (a) Cepstrum is shown as a 2D image. The spikes appear as bright spots around the center of the image; (b) cepstrum shown as a surface plot.

variance σ_v^2 of the white noise $v(n_1, n_2)$ — are not necessarily assumed to be known.

If we can assume that both the observation noise $w(n_1, n_2)$ and the image model noise $v(n_1, n_2)$ are Gaussian distributed, the log-likelihood function of the observed image, given the image model and blur parameters, can be formulated. Although the log-likelihood function can be formulated in the spatial domain, its spectral version is slightly easier to compute [13]:

$$L(\theta) = - \sum_u \sum_v \left(\log P(u, v) + \frac{|G(u, v)|^2}{P(u, v)} \right) \quad (35a)$$

where θ symbolizes the set of parameters to be estimated, i.e., $\theta = \{a_{i,j}, \sigma_v^2, d(n_1, n_2), \sigma_w^2\}$, and $P(u, v)$ is defined as

$$P(u, v) = \sigma_v^2 \frac{|D(u, v)|^2}{|1 - A(u, v)|^2} + \sigma_w^2. \quad (35b)$$

Here $A(u, v)$ is the discrete 2-D Fourier transform of $a_{i,j}$.

The objective of maximum likelihood blur estimation is now to find those values for the parameters $a_{i,j}$, σ_v^2 , $d(n_1, n_2)$ and σ_w^2 that maximize the log-likelihood function $L(\theta)$. From the perspective of parameter estimation, the optimal parameter values best explain the observed degraded image. A careful analysis of (35) shows that the maximum likelihood blur estimation problem is closely related to the identification of 2D auto-regressive moving-average (ARMA) stochastic processes [16, 13].

The maximum likelihood estimation approach has several problems that require non-trivial solutions. Actually the differentiation between state-of-the-art blur identification procedures is mostly in the way they handle these problems [11]. In the first place, some constraints must be enforced

in order to obtain a unique estimate for the point-spread function. Typical constraints are:

- the energy conservation principle, as described by equation (5b),
- symmetry of the point-spread function of the blur, i.e., $d(-n_1, -n_2) = d(n_1, n_2)$.

Secondly, the log-likelihood function (35) is highly non-linear and has many local maxima. This makes the optimization of (35) difficult, no matter what optimization procedure is used. In general, maximum likelihood blur identification procedures require good initializations of the parameters to be estimated in order to ensure converge to the global optimum. Alternatively, multi-scale techniques could be used, but no “ready-to-go” or “best” approach has been agreed upon so far.

Given reasonable initial estimates for θ , various approaches exist for the optimization of $L(\theta)$. They share the property of being iterative. Besides standard gradient-based searches, an attractive alternative exists in the form of the expectation-minimization (EM) algorithm. The EM-algorithm is a general procedure for finding maximum likelihood parameter estimates. When applied to the blur identification procedure, an iterative scheme results that consists of two steps [12, 18] (see Fig. 13):

Expectation step:

Given an estimate of the parameters θ , a restored image $\hat{f}_E(n_1, n_2)$ is computed by the Wiener restoration filter (16). The power spectrum is computed by (20b) using the given image model parameter $a_{i,j}$ and σ_v^2 .

Maximization step:

Given the image restored during the expectation step, a new estimate of θ can be computed. First, from the restored image

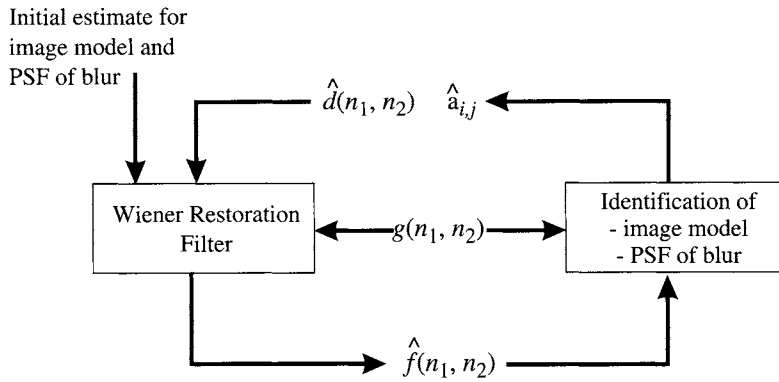


FIGURE 13 Maximum likelihood blur estimation by the EM-procedure.

$\hat{f}_E(n_1, n_2)$ the image model parameters $a_{i,j}$, σ_v^2 can be estimated directly. Secondly, from the approximate relation

$$g(n_1, n_2) \approx d(n_1, n_2) * \hat{f}_E(n_1, n_2) \quad (36)$$

and the constraints imposed on $d(n_1, n_2)$, the coefficients of the point-spread function can be estimated by standard system identification procedures [14].

By alternating the E-step and the M-step, convergence to a (local) optimum of the log-likelihood function is achieved. A particular attractive property of this iteration is that although the overall optimization is non-linear in the parameters θ , the individual steps in the EM-algorithm are entirely linear. Furthermore, as the iteration progresses, intermediate restoration results are obtained that allow for monitoring of the identification process.

In conclusion we observe that the field of blur identification has significantly less thoroughly been studied and developed than the classical problem of image restoration. Research in image restoration continues with a focus on blur identification using for instance cumulants and generalized cross-validation [11].

References

- [1] Andrews, H.C. and B.R. Hunt, *Digital Image Restoration*, Prentice Hall Inc., New Jersey, 1977.
- [2] Banham, M.R. and A.K. Katsaggelos, "Digital Image Restoration", *IEEE Signal Processing Magazine*, 14 (2), 24–41, March 1997.
- [3] Biemond, J., R.L. Lagendijk and R.M. Mersereau, "Iterative Methods for Image Deblurring", *Proceeding of the IEEE*, 78 (5), 856–883, May 1990.
- [4] Combettes, P.L., "The Foundation of Set Theoretic Estimation", *Proceeding of the IEEE*, 81, 182–208, 1993.
- [5] Galatsanos, N.P. and R. Chin, "Digital Restoration of Multi-channel Images", *IEEE Transactions on Signal Processing*, 37, 415–421, 1989.
- [6] Jeng, F. and J.W. Woods, "Compound Gauss-Markov Random Fields for Image Estimation", *IEEE Transactions on Signal Processing*, 39, 683–697, 1991.
- [7] Hunt, B.R., "The Application of Constrained Least Squares Estimation to Image Restoration by Digital Computer", *IEEE Transactions on Computers*, 2, 805–812, Sept. 1973.
- [8] Jain, A.K., "Advances in Mathematical Models for Image Processing", *Proceeding of the IEEE*, 69 (5), 502–528, May 1981.
- [9] Katsaggelos, A.K. (ed.), *Digital Image Restoration*, Springer Verlag, New York, 1991.
- [10] Katsaggelos, A.K., "Iterative Image Restoration Algorithm", *Optical Engineering*, 28 (7), 735–748, 1989.
- [11] Kundur, D. and D. Hatzinakos, "Blind Image Deconvolution: An Algorithmic Approach to Practical Image Restoration", *IEEE Signal Processing Magazine*, 13 (3), 43–64, May 1996.
- [12] Lagendijk, R.L., J. Biemond and D.E. Boekee, "Identification and Restoration of Noisy Blurred Images Using the Expectation-Maximization Algorithm", *IEEE Trans. on Acoustics, Speech and Signal Processing*, 38, 1180–1191, 1990.
- [13] Lagendijk, R.L., A.M. Tekalp and J. Biemond, "Maximum Likelihood Image and Blur Identification: A Unifying Approach", *J. Optical Engineering*, 29 (5), 422–435, 1990.
- [14] Lagendijk, R.L. and J. Biemond, *Iterative Identification and Restoration of Images*, Kluwer Academic Publishers, Boston, M.A., 1991.
- [15] Stark, H. and J.W. Woods, *Probability, Random Processes, and Estimation Theory for Engineers*, Prentice Hall, Upper Saddle River, N.J., 1986.
- [16] Tekalp, A.M., H. Kaufman, J.W. Woods, "Identification of Image and Blur Parameters for the Restoration of Non-causal Blurs", *IEEE Trans. on Acoustics, Speech and Signal Processing*, 34, 963–972, 1986.
- [17] Woods, J.W. and V.K. Ingle, "Kalman Filtering in Two-Dimensions — Further Results", *IEEE Trans. on Acoustics, Speech and Signal Processing*, 29, 188–197, 1981.
- [18] You, Y.L. and M. Kaveh, "A Regularization Approach to Joint Blur Identification and Image Restoration", *IEEE Trans. on Image Processing*, 5, 416–428, 1996.